analytical chemistry

pubs.acs.org/ac Article

# Integrating Ordered Two-Dimensional Covalent Organic Frameworks to Solid-State Nanofluidic Channels for Ultrafast and Sensitive Detection of Mercury

Xu-Qin Ran, Hai-Long Qian,* and Xiu-Ping Yan*

Cite This: *Anal. Chem.* 2022, 94, 8533−8538 Read Online

ACCESS | Metrics & More | Article Recommendations | Supporting Information

**ABSTRACT:** Grafting specific recognition moieties onto solid-state nanofluidic channels is a promising way for selective and sensitive sensing of analytes. However, the time-consuming interaction between recognition moieties and analytes is the main hindrance to the application of nanofluidic channel-based sensors in rapid detection. Here, we show the integration of ordered two-dimensional covalent organic frameworks (2D COFs) to solid-state nanofluidic channels to achieve rapid, selective, and sensitive detection of contaminants. As a proof of concept, a thiourea-linked 2D COF (JNU-3) as the recognition unit is covalently bonded on the stable artificial anodic aluminum oxide nanochannels (AAO) to fabricate a JNU-3@AAO-based nanofluidic sensor. The rapid and selective interaction of Hg(II) with the highly ordered channels of JNU-3 allows the JNU-3@AAO-based nanofluidic sensor to realize ultrafast and precise determination of Hg(II) (90 s) with a low limit of detection (3.28 fg $mL^{-1}$), wide linear range (0.01−100 pg $mL^{-1}$), and good precision (relative standard deviation of 3.8% for 11 replicate determination of 10 pg $mL^{-1}$). The developed method was successfully applied to the determination of mercury in a certified reference material A072301c (rice powder), real water, and rice samples with recoveries of 90.4−99.8%. This work reveals the great potential of 2D COFs-modified solid-state nanofluidic channels as a sensor for the rapid and precise detection of contaminants in complicated samples.

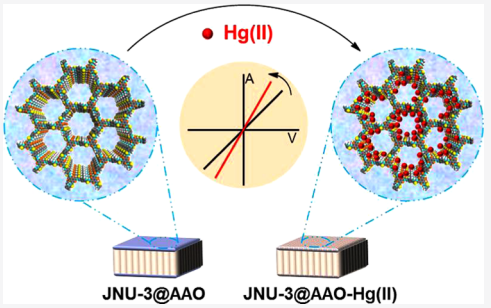




## INTRODUCTION

The growing contaminants including heavy ions, food-borne pathogens, biotoxins, veterinary drugs, pesticides, and unauthorized chemicals in the environment and food become a great threat to humans.[1−4] Therefore, establishing analytical platforms to achieve effective monitoring and precise detection of hazardous materials in the real world is of great indispensability. Extensive technologies such as high-performance liquid chromatography or gas chromatography equipped with mass spectrometry, fluorescence sensing, and electrochemical detection have been devoted to meet the requirements of the analysis of real samples.[5−18] Even so, a rapid, sensitive, and selective platform based on portable equipment is still practically desired.

Specific recognition moiety-functionalized solid-state nanofluidic channels have been shown to be selective and sensitive sensors for various analytes.[19−30] Steady-state current change with chemical composition, surface charge, wettability, and the diameter of the nanofluidic channel caused by even a single molecule can be efficaciously recorded, endowing nanofluidic sensors with sensitivity down to aM levels.[28,31−33] The introduction of various specific recognition moieties including aptamer, phenylboronic acid, antibodies, and functional metal−organic frameworks brings the nanofluidic channel target-specific selectivity.[34,35] However, the time-consuming interaction of the recognition moieties and the targets is a great limitation for the application of nanofluidic channel-based sensors in rapid detection.[19,36−38] Thus, promoting the kinetics for the interaction between the analyte and the recognition moiety on the nanofluidic channels is the key to overcome the limitation.

The interaction kinetics highly relates to the accessibility of the analyte and the active recognition sites on the nanofluidic channel.[39] The crystalline covalent organic frameworks (COFs) with large specific surface area, permanent pores, and ordered structure are well known with rapid kinetics for the interaction with analyte.[40,41] The inherent ordered channels make two-dimensional (2D) COFs promising as nanofluidic channels. Recently, the nanochannels of a few 2D COFs have been applied in bio-sensing, enantiomer separation, and water desalination.[42−44] However, 2D COFs nanochannels always suffer from difficult thickness control and poor mechanical stability.[45] The artificial anodic aluminum oxide

Received: April 12, 2022
Accepted: May 20, 2022
Published: June 2, 2022





https://doi.org/10.1021/acs.analchem.2c01595
*Anal. Chem.* 2022, 94, 8533−8538

nanochannel (AAO) is well known for its good mechanical and chemical stability.[46] Therefore, the integration of 2D COFs with AAO seems promising for the fabrication of nanofluidic sensors for rapid and sensitive detection but, to the best of my knowledge, has not been explored so far.

Herein, we report the rational design of 2D COF-functionalized AAO as a nanofluidic sensor for the rapid and precise detection of contaminants. As a proof of concept, an irreversible 2D thiourea-linked COF (JNU-3) was covalently bonded on the outer surface of AAO to obtain the JNU-3-functionalized AAO (JNU-3@AAO), while an important pollutant Hg(II) was selected as the analyte. The strong specific affinity of thiourea-linked JNU-3 to Hg(II) with highly ordered channels would promote the selectivity and kinetics for JNU-3@AAO to recognize Hg(II). Thus, the JNU-3@AAO-based sensor was developed for sensitive and ultrafast detection of mercury in real water and rice samples. This work reveals the high potential of 2D COFs-modified nanofluidic channels for rapid and precise sensing of contaminants in complicated samples.

## EXPERIMENTAL SECTION

**Materials and Chemicals.** AAO (30 ± 5 nm OD. × 60 ± 5 μm thickness × ca. 2.8 × $10^{10}$ $cm^{-2}$ channel density) was obtained from PuYuan (Hefei, China). (3-Aminopropyl)-triethoxysilane (APTES), 1,2-dichloro-benzene (*o*-DCB), and *N*,*N*-dimethylacetamide (DMAC) were from Aladdin (Shanghai, China). Nitric acid ($HNO_3$), hydrochloric acid (HCl), methanol (MeOH), ethanol (EtOH), acetone, trifluoroacetic acid (TFA), *N*,*N*-dimethylformamide (DMF), (hydroxymethyl)-methyl aminomethane (Tris, 99%), NaCl, $FeCl_3$, $CuSO_4 \cdot 3H_2O$, $CrCl_3 \cdot 6H_2O$, $CdN_2O_6 \cdot 4H_2O$, $ZnCl_2$, and $Pb(NO_3)_2$ were from Sinopharm (Shanghai, China). 1,3,5-Triformylphloroglucinol (Tp) and 1,4-phenylenebis-(thiourea) (Pa-S) were from Yanshen Technology (Jilin, China). Stock standard solution of Hg(II) (1 g $L^{-1}$) and a certified rice powder (A072301c) were from Meizheng Bio-tech (Beijing, China). All reagents used were at least of analytical grade. Ultrapure water was from Wahaha Co. (Hangzhou, China). All glass containers and digestion tubes were soaked in an acid solution ($HNO_3/H_2O$ = 1/4, v/v) for 24 h and then cleaned with ultrapure water.

**Instrumentation.** Powder X-ray diffraction (PXRD) patterns were recorded on a D2 PHASER X-ray diffractometer (Bruker, German) using Cu K$\alpha$ radiation ($\lambda$ = 1.5418 Å) with a scanning speed of 8° $min^{-1}$ and a step size of 0.05° in 2$\theta$. Scanning electron microscopy (SEM) images were recorded on an S-3500N microscope (Hitachi, Japan). A Nicolet IR IS10 spectrometer (Nicolet) with pure KBr pellets was applied to record the Fourier transform infrared (FTIR) spectra. X-ray photoelectron spectroscopy (XPS) experiments were performed on Axis Supra (Kratos, U.K.). The $\zeta$-potentials were determined on a Nano ZS Zetasizer with a 633 nm He−Ne laser (Malvern, U.K.). Analytical samples were digested on an ETHOS UP microwave digestion instrument (Milestone, Italy). A laboratory-built system as described in our previous work[19] was used for the detection of Hg(II).

**Preparation of the JNU-3@AAO-Based Sensor.** Typically, the amino-functionalized AAO (AAO-$NH_2$) was prepared according to our previous work.[19] For the in situ growth of JNU-3 on AAO-$NH_2$, AAO-$NH_2$ was immersed in a mixture containing DMAC (0.8 mL), *o*-DCB (0.2 mL), 3 M TFA (0.1 mL), Tp (0.075 mmol), and Pa-S (0.112 mmol) at room temperature (RT) for 3 days, then rinsed with DMF and MeOH, and vacuum-dried at RT to obtain JNU-3@AAO.

**Sample Digestion.** Real water and rice samples were collected locally. Typically, rice samples were pulverized before digestion. Water sample (0.3 mL) or rice sample (0.1 g) was mixed with 5 mL of $HNO_3$ in digestion tubes and digested on the microwave digestion instrument based on the recommended procedures (Table S1). The obtained digestion solution was transferred to a small beaker and then heated to remove $HNO_3$ at 100 °C on a temperature-controlled electric hot plate. The residual solution was adjusted to pH 6.5 with Tris solution (3 M, pH 10.6) and then made up to 10 mL with ultrapure water for further use.

**Detection of Hg(II).** Typically, one piece of JNU-3@AAO was immersed in the standard solution of Hg(II) or the prepared sample solution (40 μL) for 90 s and thoroughly rinsed with the testing solution (Tris-HCl buffer with 200 μM NaCl at pH 7.0) to obtain Hg(II)-bounded JNU-3@AAO (JNU-3@AAO-Hg). Then, JNU-3@AAO or JNU-3@AAO-Hg with an effective area of 2.5 $mm^2$ was placed in the middle of the flow cell filled with 150 μL of testing solution. *I*−*V* curves were obtained in a scanning voltage range of −1 to 1 V with a scanning speed of 10 mV $s^{-1}$.

## RESULTS AND DISCUSSION

**Fabrication and Characterization of JNU-3@AAO.** The design and fabrication of JNU-3@AAO via in situ growth are shown in Figure 1. The highly ordered JNU-3 allows the rapid

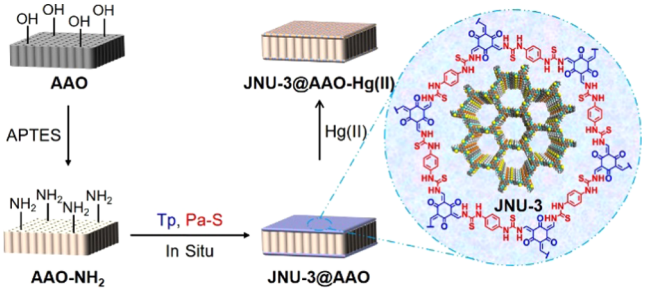


**Figure 1.** Schematic illustration of JNU-3@AAO-based nanofluidic sensor for the detection of Hg(II).

interaction of JNU-3@AAO and Hg(II). The specific affinity of the thiourea group in JNU-3 for Hg(II)[47] would cause the selective change of surface charge on JNU-3@AAO in the presence of Hg(II), allowing the ultrafast and sensitive detection of Hg(II).

Room-temperature synthesis of JNU-3 was developed via the utilization of TFA as the catalyst to facilitate the in situ growth of JNU-3 on the AAO (Figures S1−S5). AAO was modified with APTES to obtain AAO-$NH_2$. Then, the amino group of AAO-$NH_2$ further reacted with the mixture of Tp and Pa-S via the Schiff base reaction to get JNU-3@AAO.

SEM images directly show the surface change of AAO with modification. Although the color of the nanochannel showed no obvious change after the reaction of APTES, the pores of AAO-$NH_2$ became smoother than the original AAO (Figure S6). In contrast, the color of the nanochannel changed from white to dark orange (Figure S7) and dense JNU-3-like porous polymers appeared on the surface of AAO-$NH_2$ after reaction with the COF monomer (Figure S8), indicating the successful growth of JNU-3.


https://doi.org/10.1021/acs.analchem.2c01595
Anal. Chem. 2022, 94, 8533−8538

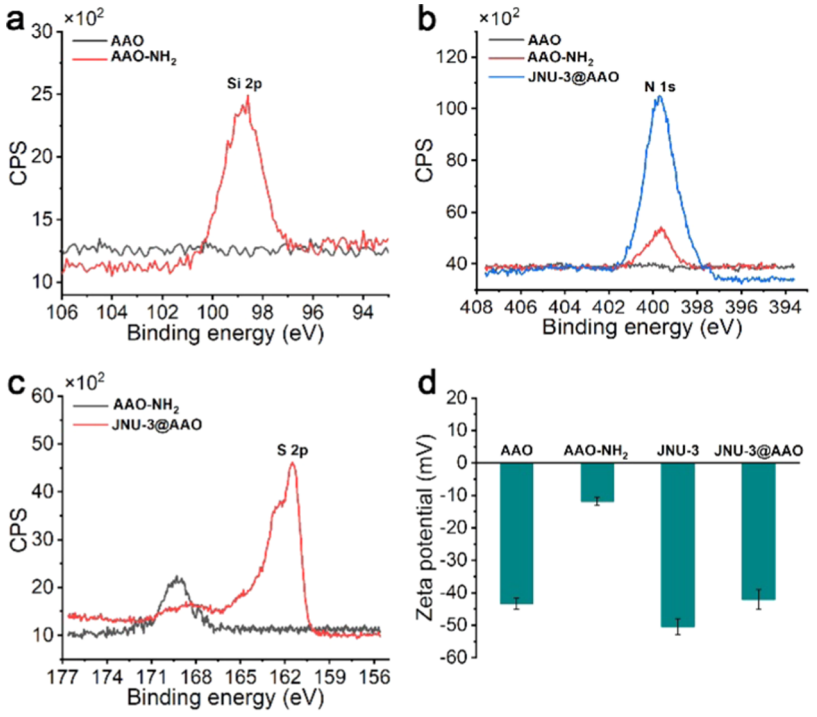


**Figure 2.** XPS spectra of different AAO: (a) Si 2p; (b) N 1s; (c) S 2p. (d) ζ-Potential of AAO, AAO-$NH_2$, JNU-3, and JNU-3@AAO.

The amount of bonded JNU-3 could be controlled with the concentration of the COF monomer. The color of the solid-state nanochannel got darker as the concentration of Tp increased from 0.05 to 0.1 mol $L^{-1}$ ($n_{Tp}/n_{Pa\text{-}S}$ = 2/3) (Figure S7). SEM image shows the insufficiency of 0.05 mol $L^{-1}$ of Tp for the preparation of JNU-3@AAO due to many uncovered original solid channels (Figure S8b). The obtained JNU-3 uniformly covered all of the channels when the concentration of Tp increased to 0.075 mol $L^{-1}$ (Figure S8c). Further increase of Tp to 0.1 mol $L^{-1}$ made the reaction tube fully filled with COF, decreasing the reproducibility of JNU-3@AAO. The reproducibility of the JNU-3@AAO prepared with different concentrations of Tp (0.05−0.1 mol $L^{-1}$) was further investigated via monitoring the $I$−$V$ curves of the randomly selected 11 pieces of JNU-3@AAO. The largest relative standard deviation (RSD) further demonstrated the low reproducibility of JNU-3@AAO prepared with Tp of 0.1 mol $L^{-1}$ (Table S2). Therefore, JNU-3@AAO prepared with Tp of 0.075 mol $L^{-1}$, which gave the best RSD, was selected for further use (Table S2).

The preparation of JNU-3@AAO was confirmed by XPS (Figure 2a−c). AAO-$NH_2$ gave evident peaks of N 1s and Si 2p appeared in its XPS spectra, demonstrating the introduction of the amino group (−$NH_2$) from APTES. Furthermore, the peak of S 2p in the XPS spectra of JNU-3@AAO proved the growth of JNU-3 on AAO-$NH_2$.

The change of contact angle and ζ-potential also proved the synthetic process of JNU-3@AAO (Figure 2d). The introduction of −$NH_2$ with a positive charge had the ζ-potential change from −43.3 ± 1.8 to −11.8 ± 1.3 eV. After in situ reaction of Tp and Pa-S, the ζ-potential of JNU-3@AAO dropped to −42.1 ± 3.1 eV due to the negative charge of JNU-3 (−50.4 ± 2.5 eV). The alkyl chain of APTES led to the increase in contact angle from 17.2 ± 1.4° to 35.1 ± 0.6°. The contact angle further increased to 49.5 ± 1.9° after the reaction of Tp and Pa-S, owing to the less hydrophilicity of JNU-3 (Figure S9).

To check the crystallinity of the grown JNU-3, the PXRD patterns of JNU-3@AAO and AAO-$NH_2$ were compared (Figure S10). AAO-$NH_2$ showed no PXRD peaks, whereas JNU-3@AAO gave two obvious characteristic peaks of JNU-3 at 3.50° and 5.99°, indicating the crystallinity of JNU-3 on AAO-$NH_2$. Furthermore, JNU-3@AAO was a highly stable sensor due to no evident change in its $I$−$V$ curve in 9 days (Figure S11).

**Sensing Conditions.** The effect of pH on the current increase rate ($(I - I_0)/I_0$) of JNU-3@AAO-Hg was first investigated in the range of 0−7. The $(I - I_0)/I_0$ increased with pH from 0 to 6 (Figure 3a) due to the competition of $H^+$ on the interaction of Hg(II) and JNU-3.[48] Further increase of pH from 6 to 7 led to no obvious increase of $(I - I_0)/I_0$ (Figure 3b). pH 6.5 was thus chosen for sensing. The kinetics for the interaction of Hg(II) and JNU-3@AAO affected sensing time. A study on the effect of time on $(I - I_0)/I_0$ revealed that 90 s was sufficient for the interaction of Hg(II) and JNU-3 (Figure 3c). The fast kinetics was attributed to the high ordered channels of JNU-3 for convenient accessibility of the analyte and greatly benefited rapid sensing.

**Analytical Performance.** The above-mentioned optimal conditions were used to develop a JNU-3@AAO-based analytical method for the determination of Hg(II). $(I - I_0)/I_0$ linearly increased with the logarithm of Hg(II) concentration from 0.01 to 100 pg $mL^{-1}$ (Figures 3d,e and S12). The detection limit (3 s) of the developed JNU-3@AAO-based analytical method was 3.28 fg $mL^{-1}$. The RSD for 11 replicate determinations of Hg(II) at 10 pg $mL^{-1}$ was 3.8%, indicating the good precision of the developed method. The proposed JNU-3@AAO-based sensor gave much lower detection limits and faster kinetics than other sensors for Hg(II), showing its superiority in sensitivity and efficiency (Table S3). The better detection limit and linear range of JNU-3@AAO ($C_{Tp}$ 0.075


https://doi.org/10.1021/acs.analchem.2c01595
Anal. Chem. 2022, 94, 8533−8538

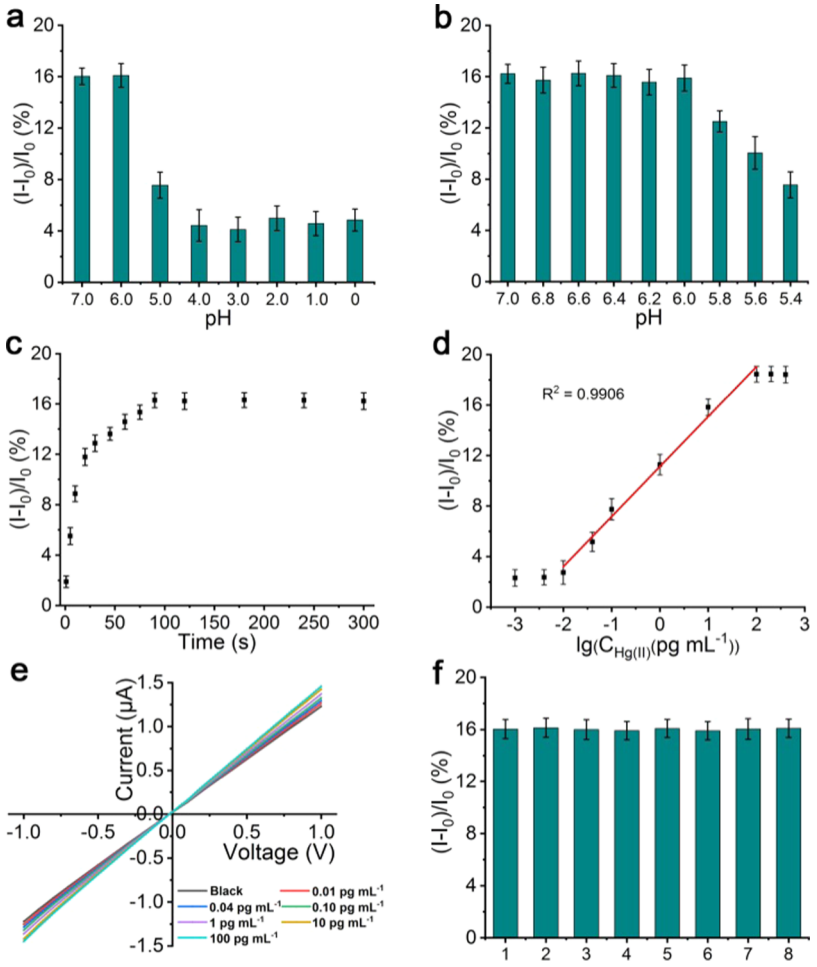


**Figure 3.** Effects of pH (a, b) and time (c) on $(I - I_0)/I_0$ of the JNU-3@AAO sensor interacted with 10 pg mL$^{-1}$ Hg(II). (d) Calibration plot of $(I - I_0)/I_0$ against the logarithm of Hg(II) concentration (0.01−100 pg mL$^{-1}$). (e) $I$−$V$ curves of JNU-3@AAO sensor interacted with different concentrations of Hg(II). (f) Effects of mixed ions (100 pg mL$^{-1}$ each) on the determination of Hg(II) (10 pg mL$^{-1}$) in aqueous solution (pH 6.5). (1, Hg(II); 2, Hg(II) + Pb(II); 3, Hg(II) + Cd(II); 4, Hg(II) + Cu(II); 5, Hg(II) + Cr(III); 6, Hg(II) + Zn(II); 7, Hg(II) + Fe(III) 8, Hg(II) + Pb(II) + Cd(II) + Cu(II) + Cr(III) + Zn(II) + Fe(III)).

mol L$^{-1}$) than JNU-3@AAO ($C_{Tp}$ 0.05 mol L$^{-1}$) further confirmed the suitability of 0.075 mol L$^{-1}$ Tp for the preparation JNU-3@AAO (Table S4).

**Selectivity.** To evaluate the selectivity of the developed JNU-3@AAO sensor for Hg(II), the anti-interference experiment was performed in real water and rice samples. The response of $(I - I_0)/I_0$ to Hg(II) (10 pg mL$^{-1}$) was evidently higher than that to the interfering ions (Pb(II), Cd(II), Cu(II), Cr(III), Zn(II), and Fe(III)) even in 10 times higher concentration (Figures S13 and S14). Moreover, the presence of these interfering ions (100 pg mL$^{-1}$) did not cause an obvious change of $(I - I_0)/I_0$ for Hg(II) (10 pg mL$^{-1}$) (Figures 3f and S15). The recoveries of 10 pg mL$^{-1}$ Hg(II) spiked in aqueous solution (pH 6.5) in the presence of these interfering ions (100 pg mL$^{-1}$ each) ranged from 96.3 to 101.7% (Table S5). In contrast, AAO-$NH_2$, which was not functionalized with JNU-3, gave no specificity to Hg(II) and the other ions even in the same concentration, demonstrating the dominant role of the proposed sensor for the selective sensing of Hg(II) (Figure S16).

**Real Sample Analysis.** To show the practicability of the developed sensing method, the JNU-3@AAO sensor was used for the determination of mercury in real samples including tap water, river water, lake water, and three kinds of rice samples. The analytical results for the determination of Hg in these samples are listed in Table 1. Only the river and lake water samples gave detectable Hg values of 0.019 ± 0.002 and 0.014 ± 0.005 μg L$^{-1}$, respectively. The recoveries of 0.15 μg L$^{-1}$

**Table 1. Determination of Mercury in Water and Rice Samples ($n$ = 3)**

| samples | spiked Hg | determined Hg (mean ± $s$) | recovery (%) (mean ± $s$) |
|---|---|---|---|
| tap water | 0 | ND[a] | |
| | 0.15 μg L$^{-1}$ | 0.148 ± 0.007 μg L$^{-1}$ | 98.3 ± 4.3 |
| river water | 0 | 0.019 ± 0.002 μg L$^{-1}$ | |
| | 0.15 μg L$^{-1}$ | 0.169 ± 0.009 μg L$^{-1}$ | 99.8 ± 6.4 |
| lake water | 0 | 0.014 ± 0.005 μg L$^{-1}$ | |
| | 0.15 μg L$^{-1}$ | 0.157 ± 0.012 μg L$^{-1}$ | 95.3 ± 4.7 |
| rice 1 | 0 | ND | |
| | 0.45 μg kg$^{-1}$ | 0.431 ± 0.021 μg kg$^{-1}$ | 95.7 ± 4.6 |
| rice 2 | 0 | ND | |
| | 0.45 μg kg$^{-1}$ | 0.427 ± 0.016 μg kg$^{-1}$ | 94.9 ± 3.5 |
| rice 3 | 0 | ND | |
| | 0.45 μg kg$^{-1}$ | 0.407 ± 0.013 μg kg$^{-1}$ | 90.4 ± 2.9 |

[a]ND: not detected.



https://doi.org/10.1021/acs.analchem.2c01595
Anal. Chem. 2022, 94, 8533−8538

Hg(II) spiked in water samples and 0.45 $\mu g\ kg^{-1}$ Hg(II) spiked in rice samples were in the range of 90.4−99.8% (Table 1). Furthermore, the mercury in the certified reference rice (A072301c) measured by our method was 41.62 ± 0.01 $\mu g\ kg^{-1}$, in good agreement with the certified value of 42.000 ± 0.009 $\mu g\ kg^{-1}$. The results proved the high potential and accuracy of the proposed JNU-3@AAO nanochannel sensor for the analysis of real samples.

## CONCLUSIONS

We have reported the design and fabrication of a thiourea-linked COF-functionalized AAO as a nanofluidic sensor for the detection of Hg(II). The JNU-3 containing rich thiourea was covalently bonded on the AAO as specific recognition moiety for Hg(II) via in situ growth to develop a JNU-3@AAO sensor. The ordered channels of JNU-3 also greatly promoted the kinetics of the interaction of Hg(II) and JNU-3@AAO, allowing ultrafast and sensitive determination of mercury in complicated real samples. This work reveals the high potential of the integration of 2D COFs to solid-state nanofluidic channels in the rapid and precise determination of contaminants in food and environment samples.

## ASSOCIATED CONTENT

### Supporting Information

The Supporting Information is available free of charge at https://pubs.acs.org/doi/10.1021/acs.analchem.2c01595.

Method and illustration for the synthesis of JNU-3; characterization of JNU-3 (experimental and simulated PXRD patterns, FTIR spectra, and SEM); characterization of modified AAO (contact angles, SEM, PXRD patterns); $I-V$ curves of JNU-3@AAO tested at different times and JNU-3@AAO-Hg with different concentrations of Hg(II); effect of other ions on the $(I - I_0)/I_0$ of JNU-3@AAO or AAO-$NH_2$; operating procedures of the microwave digestion instrument; RSD of the current for JNU-3@AAO at −1 V prepared with different concentrations of Tp; comparison of our method with previous works; and comparison of the sensing performance of JNU-3@AAO with different monomer concentrations (PDF)

## AUTHOR INFORMATION


### Corresponding Authors

**Hai-Long Qian** − *State Key Laboratory of Food Science and Technology, Jiangnan University, Wuxi 214122, China; International Joint Laboratory on Food Safety and Institute of Analytical Food Safety, School of Food Science and Technology, Jiangnan University, Wuxi 214122, China;* orcid.org/0000-0001-7554-4115; Email: hlqian@jiangnan.edu.cn

**Xiu-Ping Yan** − *State Key Laboratory of Food Science and Technology, Jiangnan University, Wuxi 214122, China; International Joint Laboratory on Food Safety, Institute of Analytical Food Safety, School of Food Science and Technology, and Key Laboratory of Synthetic and Biological Colloids, Ministry of Education, School of Chemical and Material Engineering, Jiangnan University, Wuxi 214122, China;* orcid.org/0000-0001-9953-7681; Email: xpyan@jiangnan.edu.cn

### Author

**Xu-Qin Ran** − *State Key Laboratory of Food Science and Technology, Jiangnan University, Wuxi 214122, China; International Joint Laboratory on Food Safety and Institute of Analytical Food Safety, School of Food Science and Technology, Jiangnan University, Wuxi 214122, China*

Complete contact information is available at: https://pubs.acs.org/10.1021/acs.analchem.2c01595


### Notes

The authors declare no competing financial interest.

## ACKNOWLEDGMENTS

This work was supported by the National Natural Science Foundation of China (nos. 22076066 and 22176073), the National First-class Discipline Program of Food Science and Technology (no. JUFSTR 20180301), and the Program of "Collaborative Innovation Center of Food Safety and Quality Control in Jiangsu Province".

## REFERENCES


(1) Xiao, X.; Hu, S.; Lai, X.; Peng, J.; Lai, W. *Trends Food Sci. Technol.* **2021**, *111*, 68−88.
(2) Zhang, Z.; Lou, Y.; Guo, C.; Jia, Q.; Song, Y.; Tian, J.-Y.; Zhang, S.; Wang, M.; He, L.; Du, M. *Trends Food Sci. Technol.* **2021**, *118*, 569−588.
(3) Redan, B. W.; Jackson, L. S. *J. Agric. Food Chem.* **2020**, *68*, 12773−12775.
(4) Su, Z.; Li, T.; Wu, D.; Wu, Y.; Li, G. *J. Agric. Food Chem.* **2022**, *70*, 458−469.
(5) Jarujamrus, P.; Chawengkirttikul, R.; Shiowatana, J.; Siripinyanond, A. *J. Anal. At. Spectrom.* **2012**, *27*, 884−890.
(6) Aiko, V.; Mehta, A. *J. Biosci.* **2015**, *40*, 943−954.
(7) Flores Kim, J.; McCleary, N.; Nwaru, B. I.; Stoddart, A.; Sheikh, A. *Allergy* **2018**, *73*, 1609−1621.
(8) Lv, M.; Liu, Y.; Geng, J.; Kou, X.; Xin, Z.; Yang, D. *Biosens. Bioelectron.* **2018**, *106*, 122−128.
(9) Huang, L.; Sun, D. W.; Pu, H.; Wei, Q. *Compr. Rev. Food Sci. Food Saf.* **2019**, *18*, 1496−1513.
(10) Berlina, A. N.; Zherdev, A. V.; Dzantiev, B. B. *Crit. Rev. Anal. Chem.* **2019**, *49*, 209−223.
(11) Li, J.; Zhao, X.; Chen, L.-J.; Qian, H.-L.; Wang, W.-L.; Yang, C.; Yan, X.-P. *Anal. Chem.* **2019**, *91*, 13191−13197.
(12) Shi, X.; Wei, W.; Fu, Z.; Gao, W.; Zhang, C.; Zhao, Q.; Deng, F.; Lu, X. *Talanta* **2019**, *194*, 809−821.
(13) Fu, W.-J.; Peng, Z.-X.; Dai, Y.; Yang, Y.-F.; Song, J.-Y.; Sun, W.; Ding, B.; Gu, H.-W.; Yin, X.-L. *Spectrochim. Acta, Part A* **2022**, *265*, No. 120392.
(14) Wang, B.-B.; Zhao, X.; Chen, L.-J.; Yang, C.; Yan, X.-P. *Anal. Chem.* **2021**, *93*, 2589−2595.
(15) Jiang, Y.-Y.; Zhao, X.; Chen, L.-J.; Yang, C.; Yin, X.-B.; Yan, X.-P. *Talanta* **2021**, *232*, No. 122395.
(16) Chen, Z.; Zhang, Y.; Yang, Y.; Shi, X.; Zhang, L.; Jia, G. *Sens. Actuators, B* **2021**, *336*, No. 129721.
(17) Jayan, H.; Pu, H.; Sun, D.-W. *Trends Food Sci. Technol.* **2020**, *95*, 233−246.
(18) Al Mughairy, B.; Al-Lawati, H. A. J. *TrAC, Trends Anal. Chem.* **2020**, *124*, No. 115802.
(19) Ran, X.-Q.; Qian, H.-L.; Yan, X.-P. *Anal. Chem.* **2021**, *93*, 14287−14292.
(20) Wang, L.; Li, H.; Shi, L.; Li, L.; Jia, F.; Gao, T.; Li, G. *Biosens. Bioelectron.* **2022**, *195*, No. 113671.
(21) Zhou, S.; Zhang, L.; Xie, L.; Zeng, J.; Qiu, B.; Yan, M.; Liang, Q.; Liu, T.; Liang, K.; Chen, P.; Kong, B. *Anal. Chem.* **2021**, *93*, 2982−2987.

(22) Li, G.; Belwal, T.; Luo, Z.; Li, Y.; Li, L.; Xu, Y.; Lin, X. *Food Chem.* **2021**, *356*, No. 129632.
(23) Chen, H.; Xu, L.; Tuo, W.; Chen, X.; Huang, J.; Zhang, X.; Sun, Y. *Anal. Chem.* **2020**, *92*, 4131−4136.
(24) Cao, J.; Zhao, X.-P.; Younis, M. R.; Li, Z.-Q.; Xia, X.-H.; Wang, C. *Anal. Chem.* **2017**, *89*, 10957−10964.
(25) Xu, X.; Hou, R.; Gao, P.; Miao, M.; Lou, X.; Liu, B.; Xia, F. *Anal. Chem.* **2016**, *88*, 2386−2391.
(26) Liu, N.; Hou, R.; Gao, P.; Lou, X.; Xia, F. *Analyst* **2016**, *141*, 3626−3629.
(27) Liu, N.; Jiang, Y.; Zhou, Y.; Xia, F.; Guo, W.; Jiang, L. *Angew. Chem., Int. Ed.* **2013**, *52*, 2007−2011.
(28) Liu, F.-F.; Zhao, X.-P.; Liao, X.-W.; Liu, W.-Y.; Chen, Y.-M.; Wang, C. *Anal. Chem.* **2020**, *92*, 5509−5516.
(29) Zhao, X.-P.; Liu, F.-F.; Hu, W.-C.; Younis, M. R.; Wang, C.; Xia, X.-H. *Anal. Chem.* **2019**, *91*, 3582−3589.
(30) Pan, M.; Cai, J.; Li, S.; Xu, L.; Ma, W.; Xu, C.; Kuang, H. *Anal. Chem.* **2021**, *93*, 4825−4831.
(31) Wu, X.; Li, Y.; Xu, H.; Chen, Y.; Mao, H.; Ma, Q.; Du, Q.; Gao, P.; Xia, F. *Anal. Chem.* **2021**, *93*, 13711−13718.
(32) Lu, S.-M.; Peng, Y.-Y.; Ying, Y.-L.; Long, Y.-T. *Anal. Chem.* **2020**, *92*, 5621−5644.
(33) Ma, Q.; Liu, T.; Xu, R.; Du, Q.; Gao, P.; Xia, F. *Anal. Chem.* **2021**, *93*, 1984−1990.
(34) Ma, Q.; Si, Z.; Li, Y.; Wang, D.; Wu, X.; Gao, P.; Xia, F. *TrAC, Trends Anal. Chem.* **2019**, *115*, 174−186.
(35) Zhang, H.; Tian, Y.; Jiang, L. *Nano Today* **2016**, *11*, 61−81.
(36) Zhao, X.-P.; Zhou, Y.; Zhang, Q.-W.; Yang, D.-R.; Wang, C.; Xia, X.-H. *Anal. Chem.* **2019**, *91*, 1185−1193.
(37) Ouyang, Q.; Tu, L.; Zhang, Y.; Chen, H.; Fan, Y.; Tu, Y.; Li, Y.; Sun, Y. *Anal. Chem.* **2020**, *92*, 14947−14952.
(38) Tu, J.; Zhou, Z.; Liu, Y.; Li, T.; Lu, S.; Xiao, L.; Xiao, P.; Zhang, G.; Sun, Z. *RSC Adv.* **2021**, *11*, 3751−3758.
(39) Karak, S.; Dey, K.; Torris, A.; Halder, A.; Bera, S.; Kanheerampockil, F.; Banerjee, R. *J. Am. Chem. Soc.* **2019**, *141*, 7572−7581.
(40) Guan, X.; Chen, F.; Fang, Q.; Qiu, S. *Chem. Soc. Rev.* **2020**, *49*, 1357−1384.
(41) Qian, H.-L.; Wang, Y.; Yan, X.-P. *TrAC, Trends Anal. Chem.* **2022**, *147*, No. 116516.
(42) Cao, L.; Liu, X.; Shinde, D. B.; Chen, C.; Chen, I. C.; Li, Z.; Zhou, Z.; Yang, Z.; Han, Y.; Lai, Z. *Angew. Chem., Int. Ed.* **2021**, *61*, No. e202113141.
(43) Yuan, C.; Wu, X.; Gao, R.; Han, X.; Liu, Y.; Long, Y.; Cui, Y. *J. Am. Chem. Soc.* **2019**, *141*, 20187−20197.
(44) Xu, L.; Shan, B.; Gao, C.; Xu, J. *J. Membr. Sci.* **2020**, *593*, No. 117398.
(45) Singh, R.; Kim, D. *ACS Appl. Mater. Interfaces* **2021**, *13*, 33437−33448.
(46) Rajeev, G.; Prieto Simon, B.; Marsal, L. F.; Voelcker, N. H. *Adv. Healthcare Mater.* **2018**, *7*, No. 1700904.
(47) Qian, H.-L.; Zhu, M.-S.; Du, M.-L.; Ran, X.-Q.; Yan, X.-P. *J. Hazard. Mater.* **2022**, *427*, No. 128156.
(48) Merrifield, J. D.; Davids, W. G.; MacRae, J. D.; Amirbahman, A. *Water Res.* **2004**, *38*, 3132−3138.




https://doi.org/10.1021/acs.analchem.2c01595
*Anal. Chem.* 2022, 94, 8533−8538